NASA Technical Paper 2007

May 1982

Pockels-Effect Cell for Gas-Flow Simulation

David Weimer

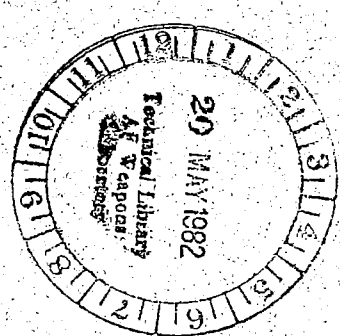

NASA

COMPLTD. 4/27/83 DM

ERRATA

NASA Technical Paper 2007

POCKELS-EFFECT CELL FOR GAS-FLOW SIMULATION

David Weimer
May 1982

Page 1: Equation (1) should be

$$n_{x'} = n_o - \frac{n_o^3}{2} r_{63} E_z$$

Page 3, reference 8: The author's name should be Ladenburg.

Issue date: February 4, 1983

NASA
Technical
Paper
2007

1982

Pockels-Effect Cell for Gas-Flow Simulation

David Weimer
Lewis Research Center
Cleveland, Ohio

NASA
National Aeronautics
and Space Administration

**Scientific and Technical
Information Branch**

Summary

A Pockels-effect flow simulator cell has been developed and tested. A $5 \times 5 \times 3$ cm KD*P electro-optic crystal with the optic axis z along the 3-cm dimension has been designed to produce an index-of-refraction gradient that is controllable with applied electric fields. Polarized light whose plane of polarization is perpendicular to z has been shown to experience a retardation proportional to E_z. Placing two pairs of 1-cm-wide electrodes on the top and bottom of the crystal (i.e., on the 5×5 cm surfaces) causes the fringing electric field E_z to be nonuniform throughout the crystal. When this is done, the index of refraction will vary throughout the crystal. The device has been calibrated by using both real-time and diffuse-illumination, double-exposure holographic interferometry. Calibration curves of fringe shift across a 5×3 cm face of the crystal versus applied voltage have been obtained. The fringe shift has the same magnitude as that generated by some common holographic methods used to visualize flows in cascades and compressors.

Introduction

Holographic flow-visualization methods at times require laboratory techniques to simulate the optical effects of gas flows and to test procedures before they are used in a large test rig. These optical effects are mainly the result of changes in the index of refraction of a gas caused by density variations. For some applications to compressor flows (ref. 1), it is desirable to have a material in which a gradient in the index of refraction can be induced in times of the order of microseconds. A Pockels effect cell has been devised in which the index gradient is controlled by the application of applied potentials.

The possible use of the electro-optic effect for producing refractive index gradients has been examined, and two possible crystals, zinc telluride and KD*P (potassium dihydrogen phosphate with 97 to 99 percent of the hydrogen replaced with deuterium), have been considered (ref. 2). This report concerns a cell made from KD*P. It is noteworthy that electric field gradients have been used with KD*P to produce a method for light beam deflection (ref. 3).

This report describes the theory, design, and performance of a KD*P Pockels-effect cell as a flow simulator. The performance of the device is studied by using real-time holographic interferometry (ref. 4). Since the Pockels-effect cell can also be used with rapid-double-exposure (ref. 5) flow visualization, its performance is also evaluated by using diffuse-illumination, double-exposure holographic interferometry (ref. 6). First, the theory and design of a Pockels-effect flow simulator are discussed.

Theory and Design of Pockels-Effect Cell

The refractive index of a crystal of KD*P can be changed by the application of an electric field along the crystal's optic axis (ref. 7). When light passes through a crystal, its propagation is determined by the index of refraction of the material and the relation of the crystal axes to the polarization direction of the light. When light with its polarization in a plane perpendicular to the optic axis passes through the KD*P crystal with no applied electric field, all parts of the wave front are subjected to the same index of refraction, independent of the direction of polarization in that plane. However, with the application of an electric field, the propagation characteristics change because of modifications to the index of refraction. For this particular application, incoming light is passed through the crystal perpendicular to the applied electric field with its plane of polarization along one of the principal axes that has been produced by the electric field in the crystal. The index characterized by this polarization depends on the electric field.

The configuration shown in figure 1 was the basis for the design of the cell. To produce a refractive index gradient in the crystal, the electrode plates are narrowed so as to produce a nonuniform field that varies with x', a coordinate along one of the principal axes (ref. 7). The index of refraction $n_{x'}$ for light polarized in the x' direction then also varies with x' and is given by

$$n_{x'} = n_o - \frac{n_o^3}{2} r_{63} E_z \tag{1}$$

where

$$n_o = n_x = n_y$$

For no applied electric field, r_{63} is the electro-optic coefficient, and E_z is the field along the optic axis (ref. 7). Note that x' is at 45° to x, one of the twofold axes of symmetry of KD*P.

The phase shift Γ experienced by the polarized wave passing through the crystal for $E_z \neq 0$ relative to the same wave when $E_z = 0$ is given by

$$\Gamma = \frac{\pi L}{\lambda_o} n_o^3 r_{63} E_z \tag{2}$$

where λ_o is the vacuum wavelength of the incident light.

Since all the light entering will travel the same distance L through the crystal, the retardation will depend on the value of the applied electric field E_z. Because of the narrow electrodes, the fringing field applied to the crystal will vary in the x' direction. Therefore, an index gradient in the x' direction will be created.

The final design of the crystal incorporated a second pair of electrodes as shown in figure 2 to produce an electric field in the $-z$ direction and thus to increase the variation in refractive index from left to right.

The crystal specifications for the cell are given in figure 2. The crystal was mounted strainfree and immersed in an index-matching fluid. The final assembly is shown with other components of a holographic setup in figure 3.

For the values $\lambda_o = 6.328 \times 10^{-7}$ m (HeNe), $n_o = 1.5$, and $r_{63} = 23.6 \times 10^{-12}$ m/V (ref. 7), a maximum of one wavelength of retardation should be observed for approximately 9500 V on one pair of electrodes. In finite fringe interferometry (ref. 8), this will appear as a shift of one fringe pair. Next, the experimental evaluation of the performance of the cell specified in figure 2 is described.

Experimental Procedure and Results

The change in the index of refraction that takes place when potentials are applied to the electrodes of the crystal was determined in the following manner: Vertically polarized radiation from a 15-mW helium-neon laser enters a holographic setup (figs. 4 and 5). Since the crystal cell is mounted most conveniently in a horizontal position, the polarization of the beam is rotated by a 1/2-wave plate so that it will also be horizontal.

The beam is split and attenuated at the first mirror, providing a reference beam and an object beam. A scatter plate (ref. 9) 7.6 cm ahead of the cell produces directional, diffused light to illuminate the cell. A hologram of the cell is produced with no voltage applied to the crystal. After the hologram plate is processed, it is repositioned in the holder and illuminated with both the object and reference beams.

The hologram is then moved slightly in the horizontal and vertical directions, producing a field of parallel interference fringes that can be localized in the plane of the scatter plate. These fringes are then photographed through an appropriate camera lens and become the reference data for fringe measurement.

Voltages are then applied to the pairs of electrodes, causing a shift in the positions of the fringes (e.g., see figs. 6 to 8). Voltages from 1 to 7 kV above ground were applied to electrodes 1 and 3 with electrodes 2 and 4 grounded and to electrodes 2 and 4 with electrodes 1 and 3 grounded.

The following procedure was used for reducing the data: In figures 6 to 8, a cut across the crystal (a fixed value of z) was selected. The position (x' coordinate) of each fringe in figures 6 to 8 was measured for the selected value of z. The x' coordinate for a particular fringe from figures 6 and 8 was compared with its position in figure 7. By noting the difference in x' and knowing the fringe spacing from figure 7 at that place in the field of view, a shift in position was computed in terms of the fringe spacing and became ΔN—the fringe shift at that point in the field. Considering the difficulties of measurement, the uncertainty in ΔN is about 1/20 of a fringe. The computed fringe shifts ΔN were plotted versus x' in figure 9 for 7 kV on electrodes 1 and 3, and in figure 10 for 7 kV on electrodes 2 and 4. Each graph is for a different value of z.

In order to see the variations in fringe shifts over the entire face of the crystal for the 7 kV applied to electrodes 1 and 3, the fringe shifts in figure 9 were plotted as constant-fringe-shift contours in the z,x' plane. These contours are shown in figure 11. A similar plot (fig. 12) of the curves in figures 10(a) to (k) gives contours of constant fringe shift for the high voltage applied to electrodes 2 and 4. The contours of constant fringe shift are then compared with the fringes obtained from diffuse-illumination, double-exposure holograms (ref. 4). For this double-exposure method, a hologram is made with a constant reference beam and two exposures of the object beam: one with applied voltage, and one with zero voltage on the cell. This produces fringes in the reconstructed image corresponding to only the change that takes place between the two exposures. The reconstructed image is photographed with a camera. These photographs for different applied voltages are shown in figures 13 and 14.

The composite fringe shifts as a function of position from figure 11 of the real-time holographic interferometry can be compared with the fringes of figure 13(a) of the double-exposure holography. Similarly, figure 12 can be compared with 14(a). Aside from perhaps a slight zero shift, the shapes of the curves agree fairly well. The composite curves (figs. 11 and 12) produce contours of fractional fringe shifts throughout the field. The double exposure produces dark fringes only for optical path differences equal to an odd multiple of a half wavelength.

When we observe the reconstruction with the eye, the fringes in figures 13 and 14 stand out markedly in the interior of the crystal. Parallax measurements have been

made on the fringes, and they are localized within a few millimeters of the middle of the crystal in agreement with the localization theory (refs. 4 and 5). A few of the measurements of their position are noted on figures 13(a) to (e). It would appear that, with the higher voltages, the localization moves slightly away from the midplane of the crystal.

Referring again to the real-time holographic interferometry, for the center cut, a special procedure was used. A mask on the centerline at the camera image divided the photograph so that half of the field was shown with zero voltage and the other half with a specified voltage. Figure 15 is an example of such a split field. This procedure puts both the disturbed and undisturbed fields on the same film and makes the measuring of the fringe shift somewhat easier.

These measurements became the calibration curves of fringe shift as a function of voltage in figure 16. It should be pointed out that the curves in figures 9, 10, and 16 have been normalized to have zero fringe at the center of the cell. The data were collected over a period of several minutes for each configuration, and on occasion the zero position would drift slightly (of the order of 1/10th of a fringe). This drift was the major experimental uncertainty.

It should also be pointed out that some dissymmetry exists between the right (3,4) and the left (1,2) sides of the crystal. The maximum shift on the right was slightly less than on the left. This shows up best in figure 16. The cause of this reduced sensitivity is possibly a lower electric field on the right side. In figure 6, there is an indication of a strong disturbance at the inside edge of electrode 4, which is perhaps causing an abnormal field in this region. This abnormality may reduce the electric field in the remainder of the crystal on the right side. In any event this dissymmetry is reproducible and the calibration can still be carried out.

A calculation of the approximate electric field was made with the four-plate electrode configuration. Assuming a uniform charge density on the plates, the x component of the field was determined (ref. 2). Since the fringe shift is directly proportional to E_z, the centerline ($z = 1.5$ cm) fringe shift should be of a similar shape. The value of the electro-optic coefficient is known only approximately, and so the electric field curves are scaled to the maximum fringe shift on each side of the crystal. This electric field approximation has been plotted in figure 16.

The parallel-fringe system used in these experiments has directional ambiguity much like that of a Mach-Zehnder interferometer (ref. 8). It is necessary to test the fringes by means of a hot iron to see which way they move. Doing this will establish their motion for a known direction of index change. Applying this test leads to the conclusion that, if the positive voltage is connected to electrodes 2 and 4 with electrodes 1 and 3 grounded, the region on the left (1,2) experiences an increase in the index of the material while the region on the right (4,3) experiences a decrease in the index. A one-fringe increase coupled with a one-fringe decrease leads to a change in index across the crystal of 1.26×10^{-5}, or a centerline gradient of

$$\frac{1.26 \times 10^{-5}}{0.05\ \text{m}} = 2.52 \times 10^{-4}/\text{m}$$

Concluding Remarks

The Pockels-cell flow simulator is intended to be used to test holographic procedures in the laboratory before they are used in a large test rig. It appears that it would be useful both in real-time and rapid-double-exposure modes of operation. The fringe shift calibration curves appear to be quite reproducible, and the cell is capable of producing index-of-refraction gradients that are comparable to those found in many flow situations.

To better understand the fringe shift pattern throughout the crystal, more exact calculations of E_z, taking into account the three-dimensional nature of the system, would be desirable.

Lewis Research Center
National Aeronautics and Space Administration
Cleveland, Ohio, December 11, 1981

References

1. Wuerker, R. F.; et al.: Application of Holography to Flow Visualization within Rotating Compressor Blade Row. NASA CR-121264, 1974.
2. Weimer, David: A Proposed Method of Generating an Index Gradient for Flow Visualization Studies. NASA Lewis-ASEE-Case Western Reserve University Summer Faculty Fellowship, 1980 Final Report D-99, prepared by the Co-Directors Joseph M. Prahl and Walter T. Olson.
3. Lotspeich, James F.: Electro-Optic Light-Beam Deflection. IEEE Spectrum, vol. 5, no. 2, Feb. 1968, pp. 45-52.
4. Vest, Charles M.: Holographic Interferometry, John Wiley & Sons, 1979, pp. 254-308.
5. Decker, Arthur J.: Fringe Localization Requirements for Three-Dimensional Flow Visualization of Shock Waves in Diffuse-Illumination, Double-Pulse Holographic Interferometry. NASA TP-1868, 1982
6. Heflinger, L. O.; Wuerker, R. F.; and Brooks, R. E.: Holographic Interferometry. J. Appl. Phys., vol. 37, no. 2, Feb. 1966, pp. 642-649.
7. Yariv, Amnon: Introduction to Optical Electronics. Second Ed. Holt, Rinehard, and Winston, Inc., 1976, pp. 245-262.
8. Ladenburg, Rudolf Walter: Physical Measurements in Gas Dynamics and Combustion. High Speed Aerodynamics and Jet Propulsion, vol. 9, Princeton University Press, 1954, p. 47.
9. Gates, J. W. C.: Holography with Scatter Plates. J. of Sci. Instr, ser. 2, vol. 1, no. 10, Oct. 1968, pp. 989-994.

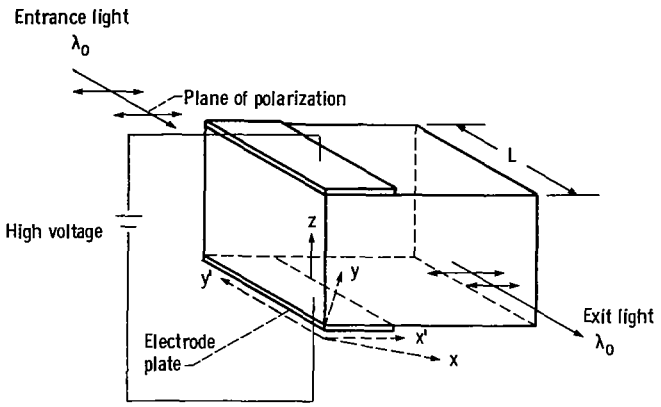

Figure 1. - Orientation of polarized light to crystal axes of KD^*P cell with optic axis along z.

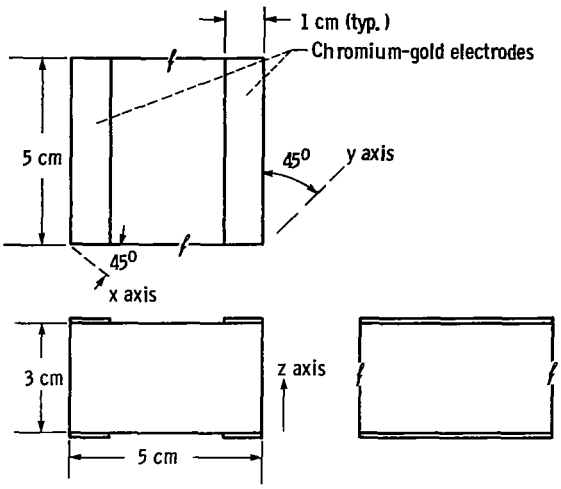

Figure 2. - Some specifications for a Pockels-effect flow simulator. KD^*P 97 to 99 percent deuterated; f faces flat to $1/4\lambda_0$; parallel to within 30 sec of arc; dimensions ±0.01 cm; highest laser optical grade.

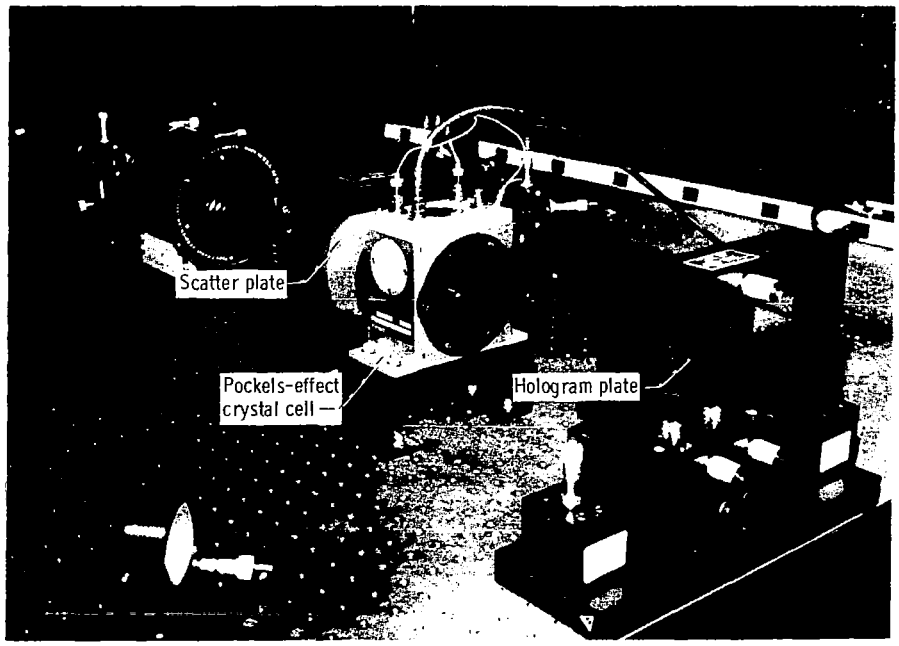

Figure 3. - Holographic interferometer setup for evaluating performance of Pockels-effect cell.

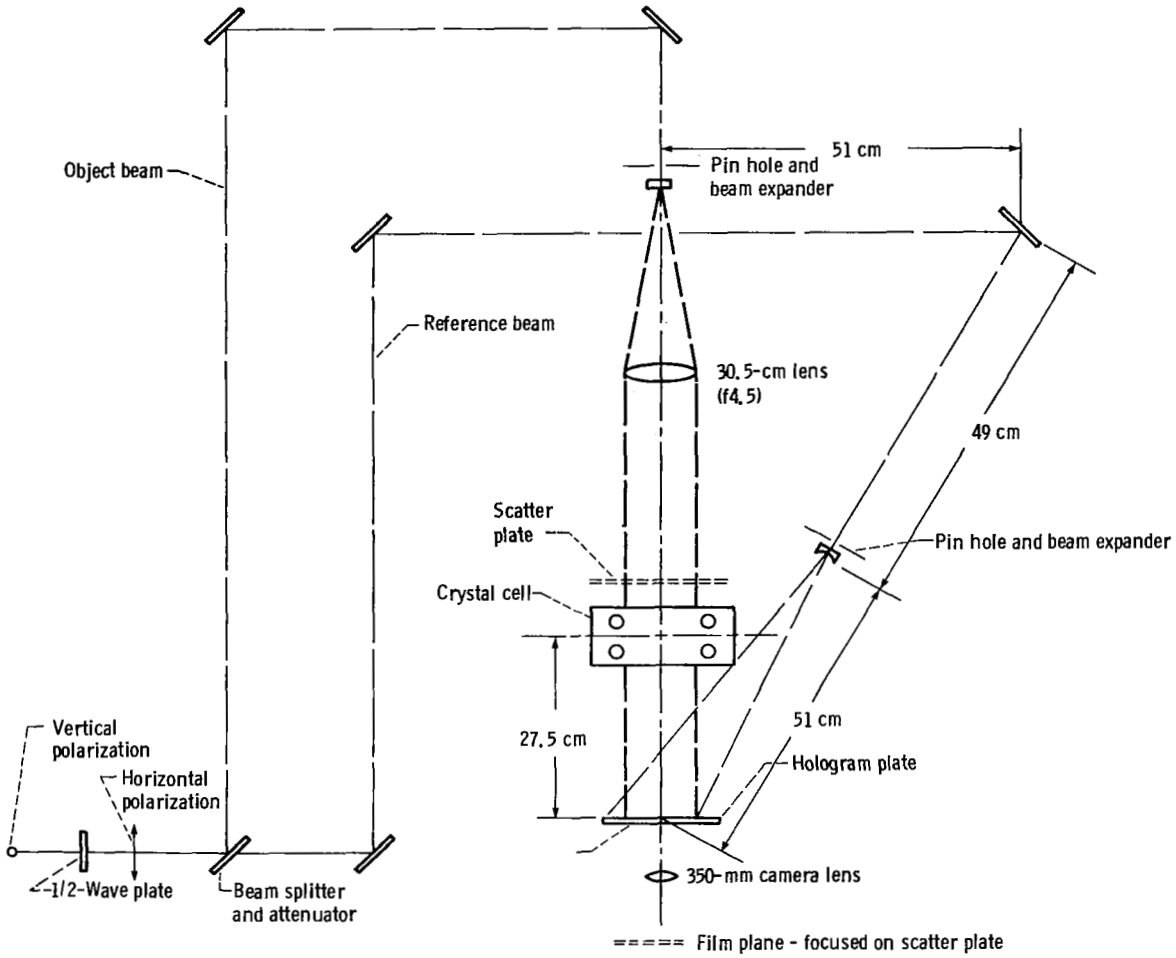

Figure 4. - Placement of optical components to produce holograms of Pockels-effect cell.

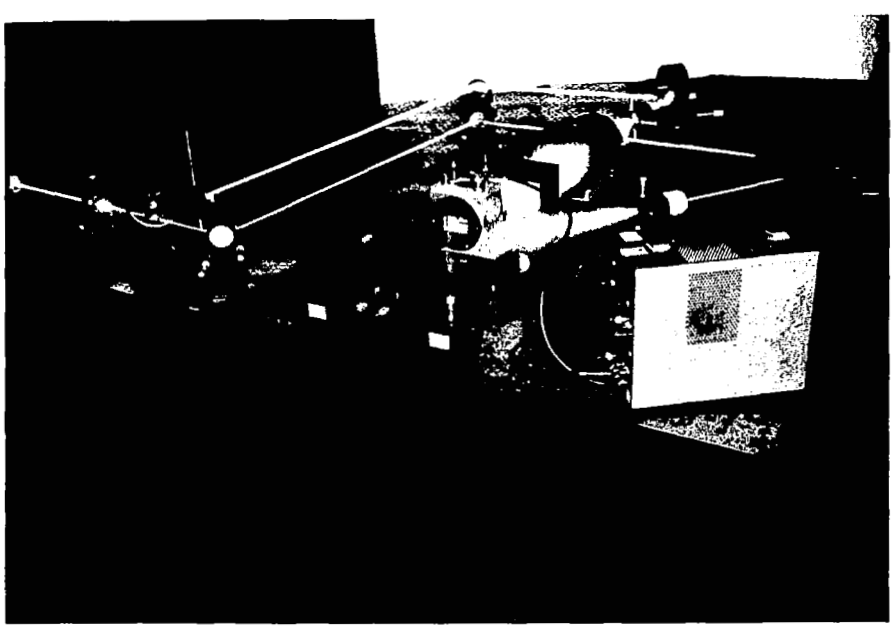

Figure 5. - Laser light paths for holograms.

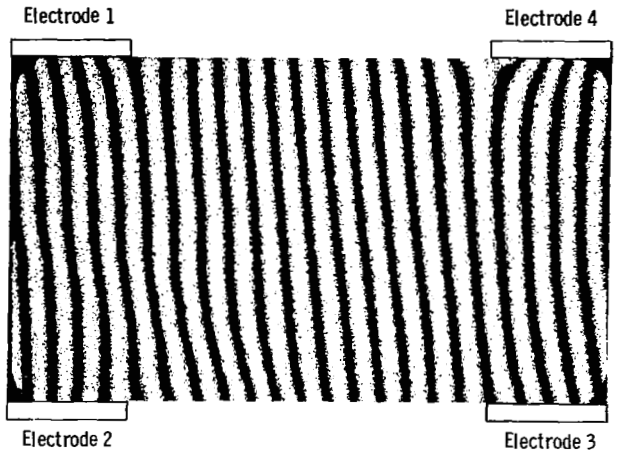

Figure 6. - Interferogram of crystal with 7 kV applied to electrodes 1 and 3, with electrodes 2 and 4 grounded.

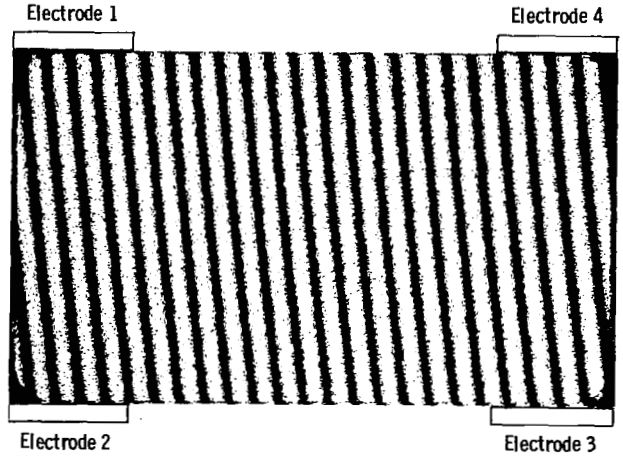

Figure 7. - Interferogram of crystal with all electrodes grounded.

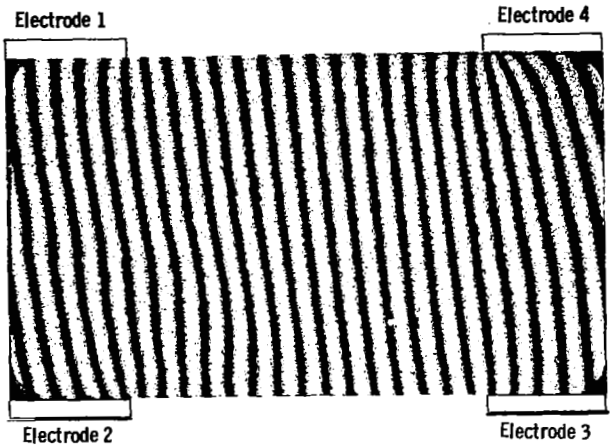

Figure 8. - Interferogram of crystal with 7 kV applied to electrodes 2 and 4, with electrodes 1 and 3 grounded.

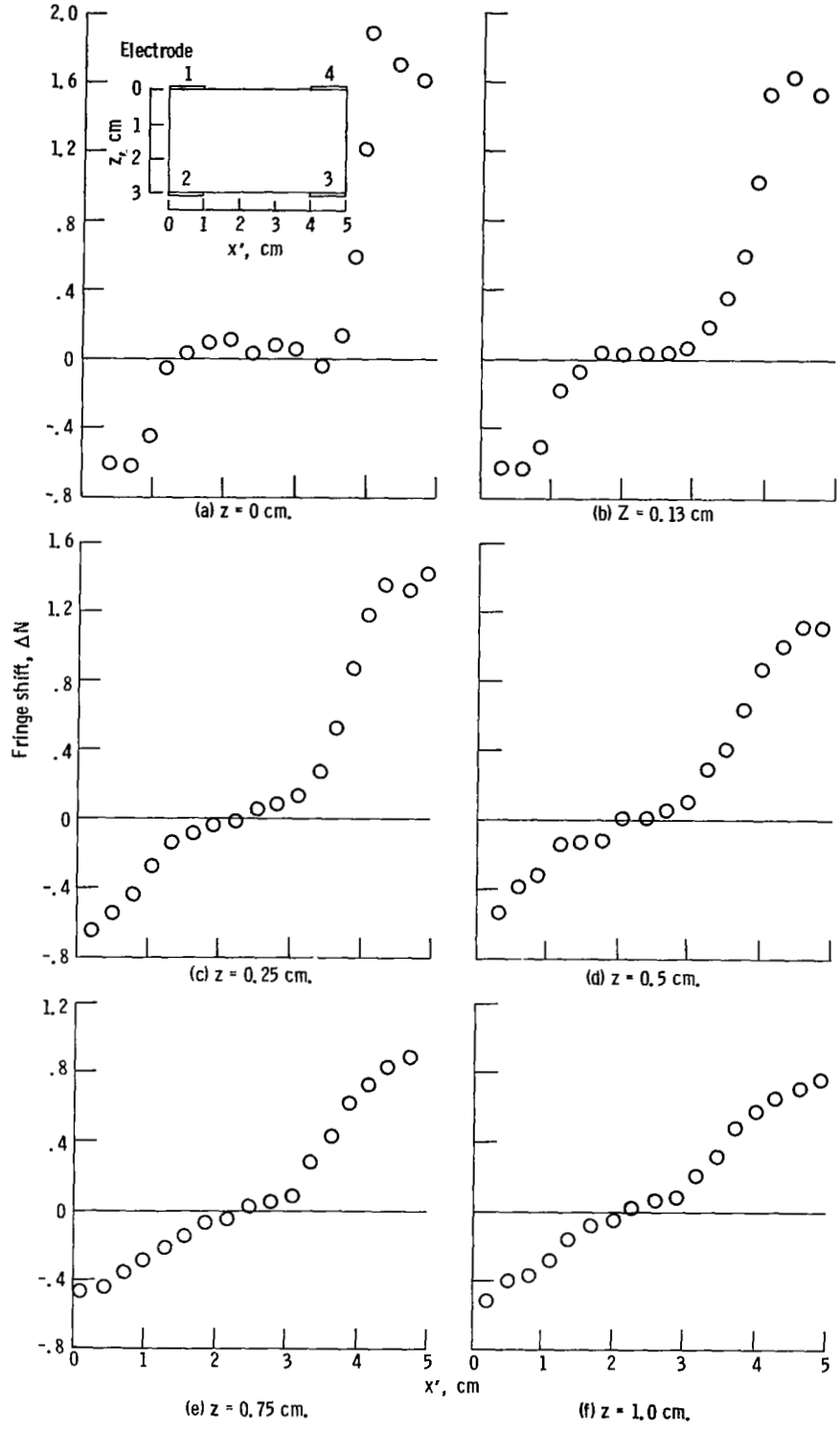

Figure 9. - Fringe shift for cut across crystal face, with potential of 7 kV on electrodes 1 and 3 and electrodes 2 and 4 grounded.

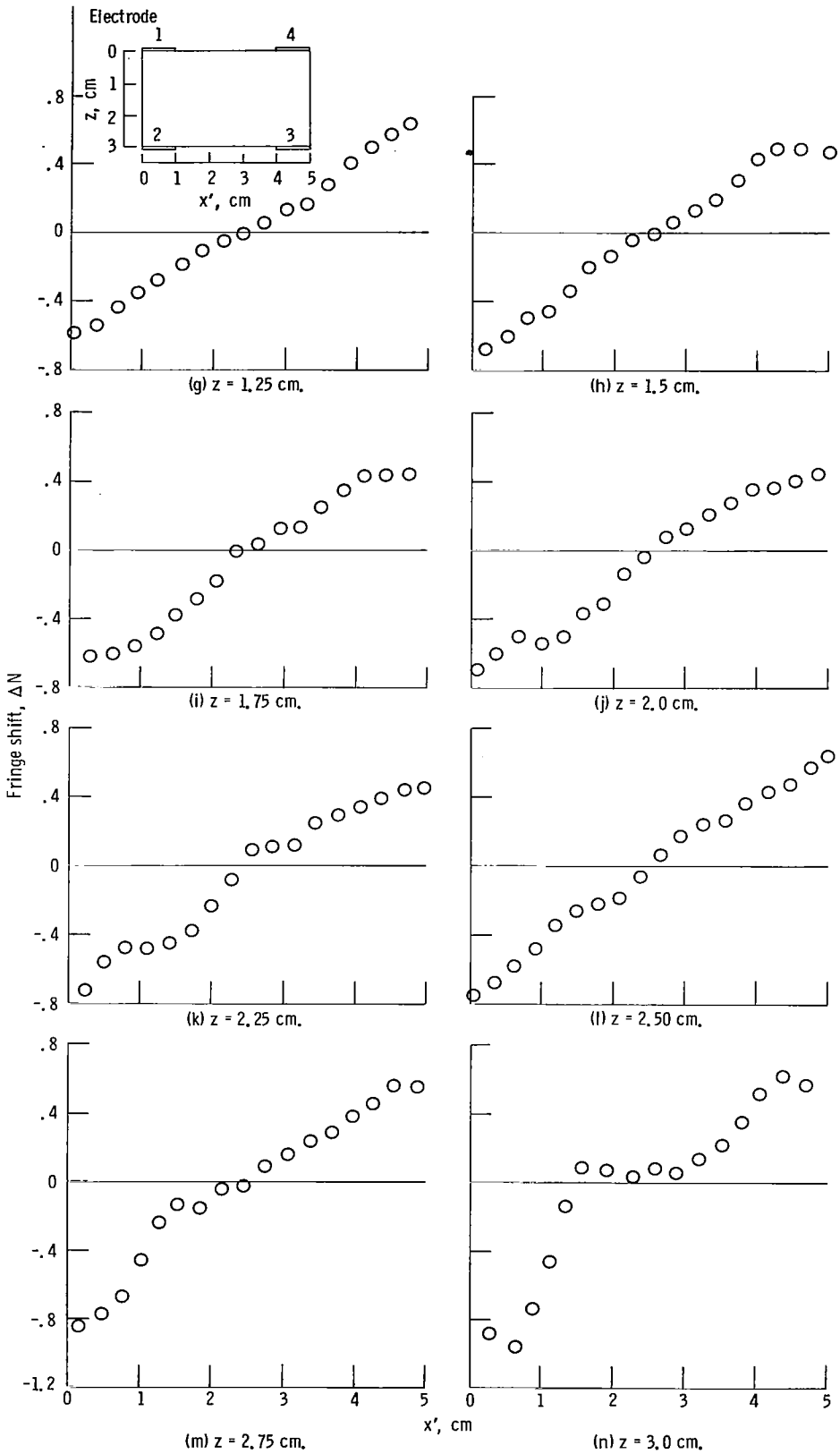

Figure 9. - Concluded.

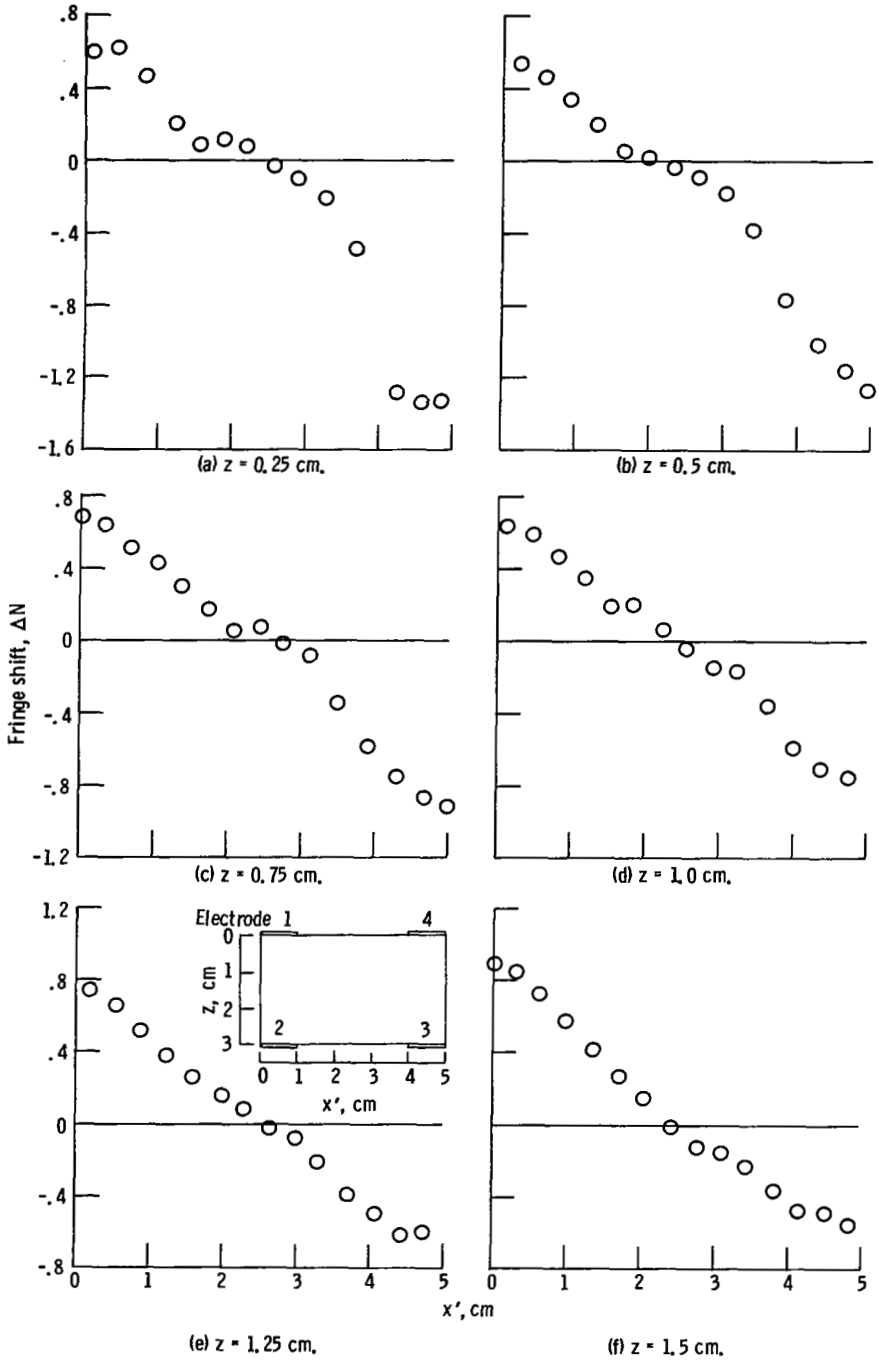

Figure 10. - Fringe shift for cut across crystal face, with potential of 7 kV on electrodes 2 and 4 and electrodes 1 and 3 grounded.

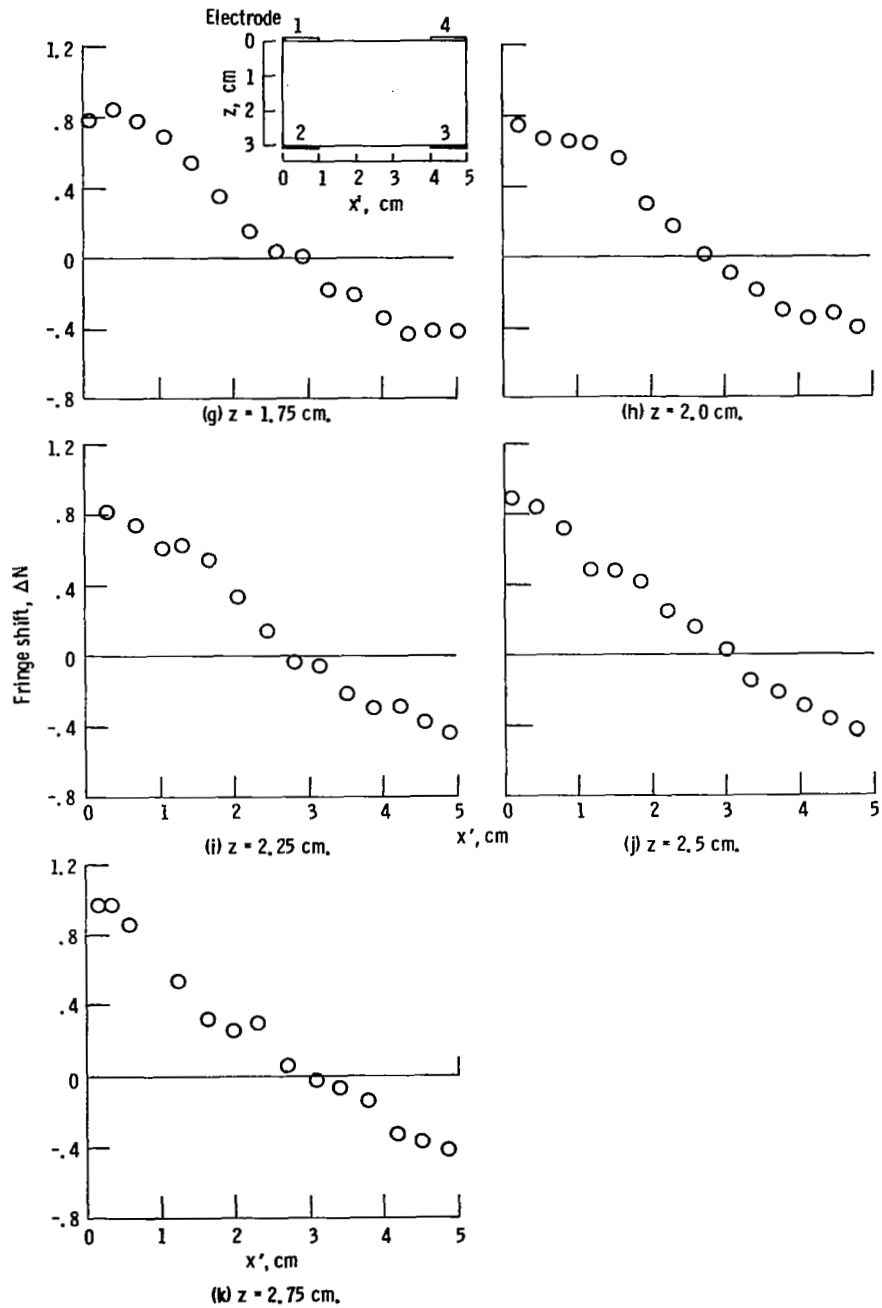

Figure 10. - Concluded.

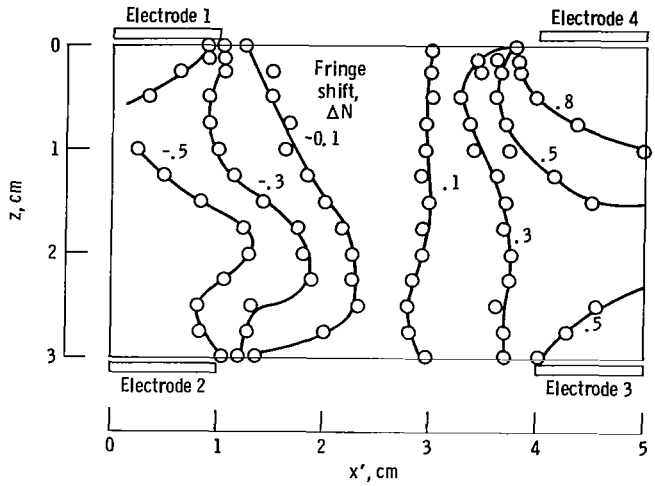

Figure 11. - Constant-fringe-shift contours for potential of 7 kV on electrodes 1 and 3, with electrodes 2 and 4 grounded.

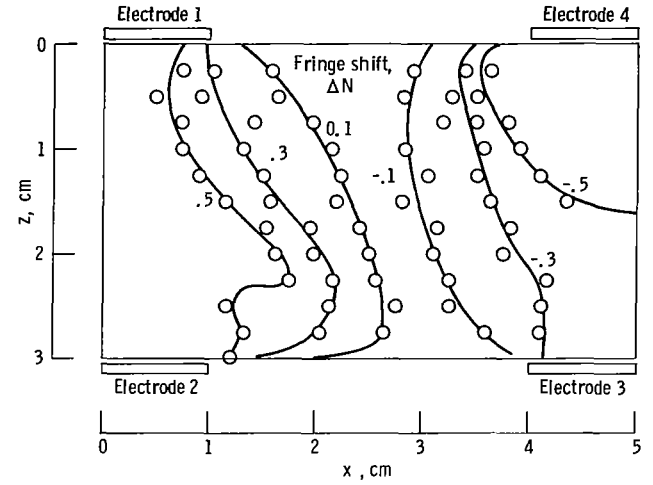

Figure 12. - Constant-fringe-shift contours for potential of 7 kV on electrodes 2 and 4, with electrodes 1 and 3 grounded.

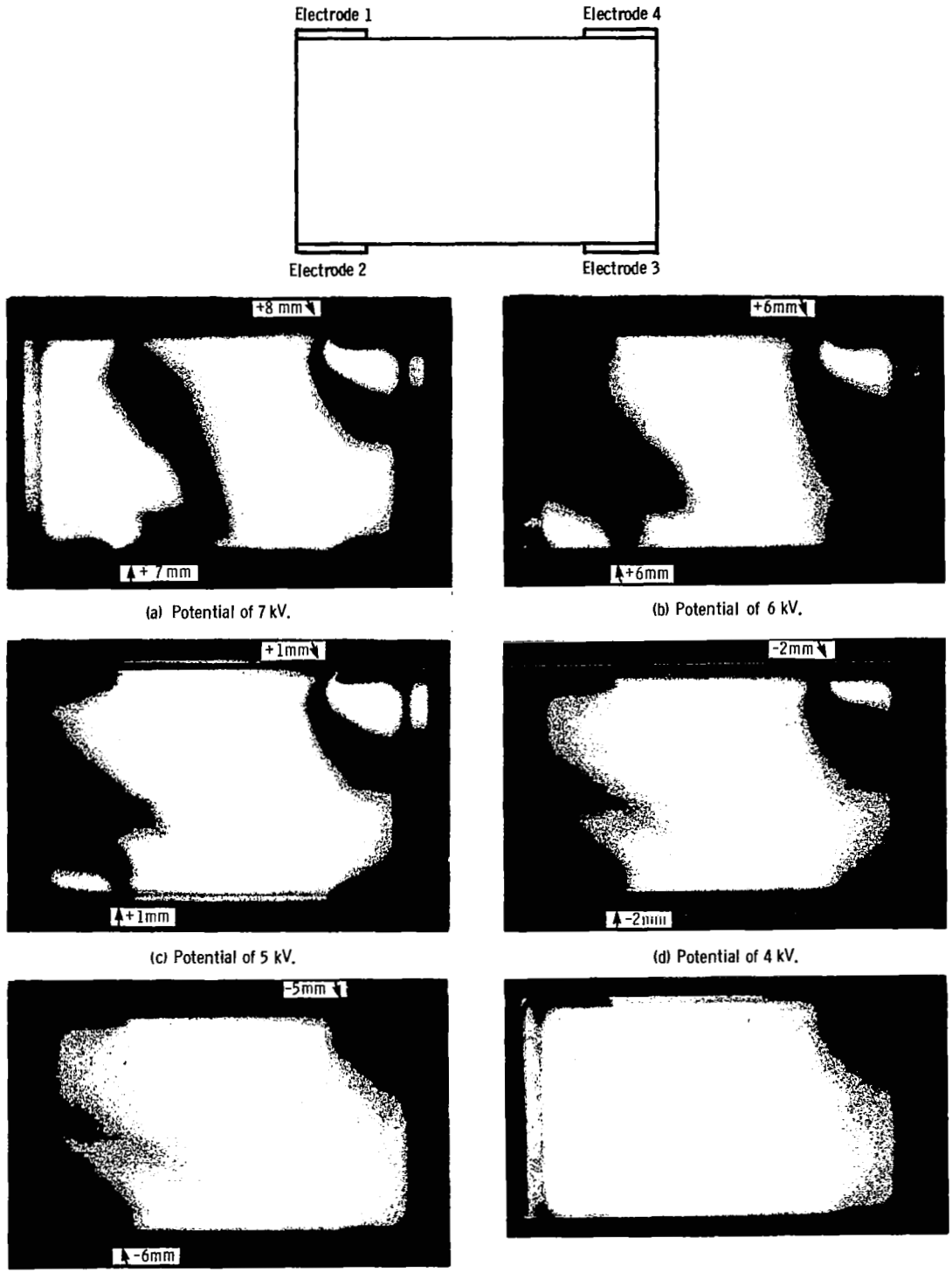

(a) Potential of 7 kV.

(b) Potential of 6 kV.

(c) Potential of 5 kV.

(d) Potential of 4 kV.

(e) Potential of 3 kV.

(f) Potential of 2 kV.

Figure 13. - Diffuse-illumination, double-exposure hologram with the high voltage on electrodes 1 and 3 and electrodes 2 and 4 grounded. (Fringes are localized at indicated positions relative to midplane of crystal, + is forward toward camera.)

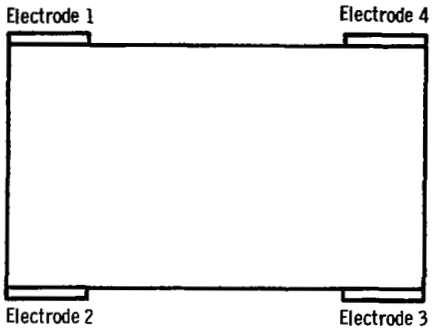

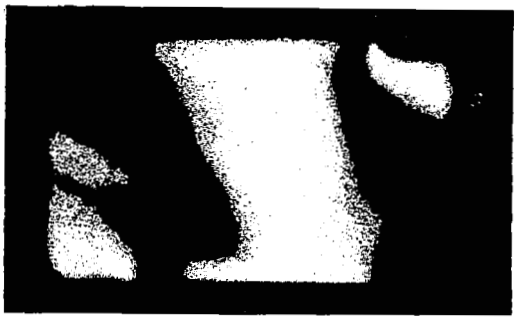

(a) Potential of 7 kV.

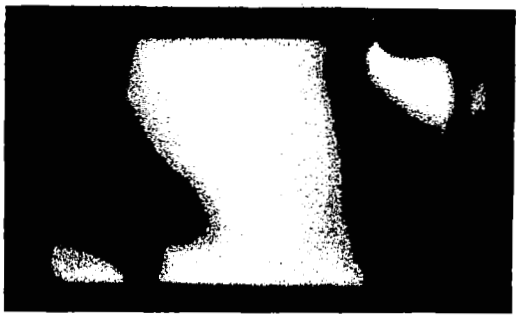

(b) Potential of 6 kV.

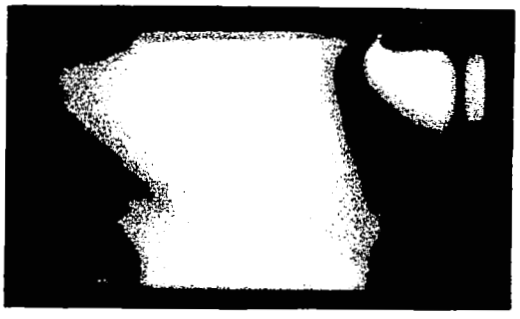

(c) Potential of 5 kV.

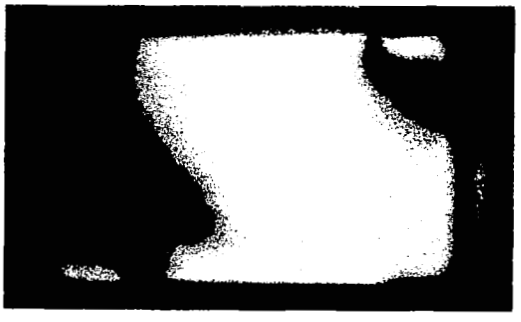

(d) Potential of 4 kV.

(e) Potential of 3 kV.

(f) Potential of 2 kV.

Figure 14. - Diffuse-illumination, double-exposure hologram with the high voltage on electrodes 2 and 4 and electrodes 1 and 3 grounded.

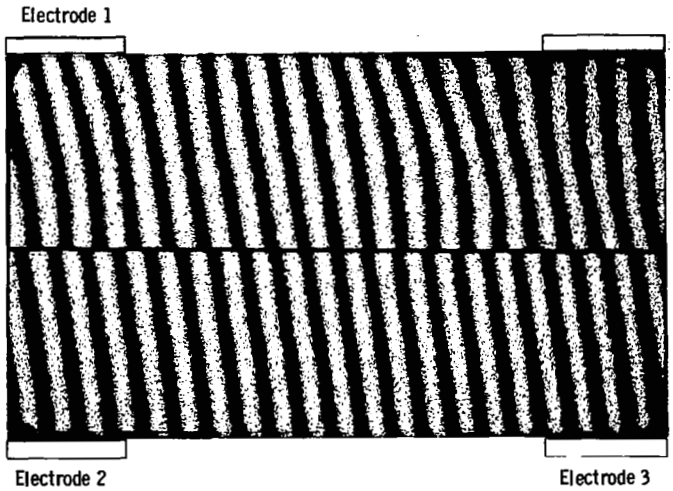

Figure 15. - Split-field interferogram. Potential of 7 kV on electrodes 1 and 3, with electrodes 2 and 4 grounded.

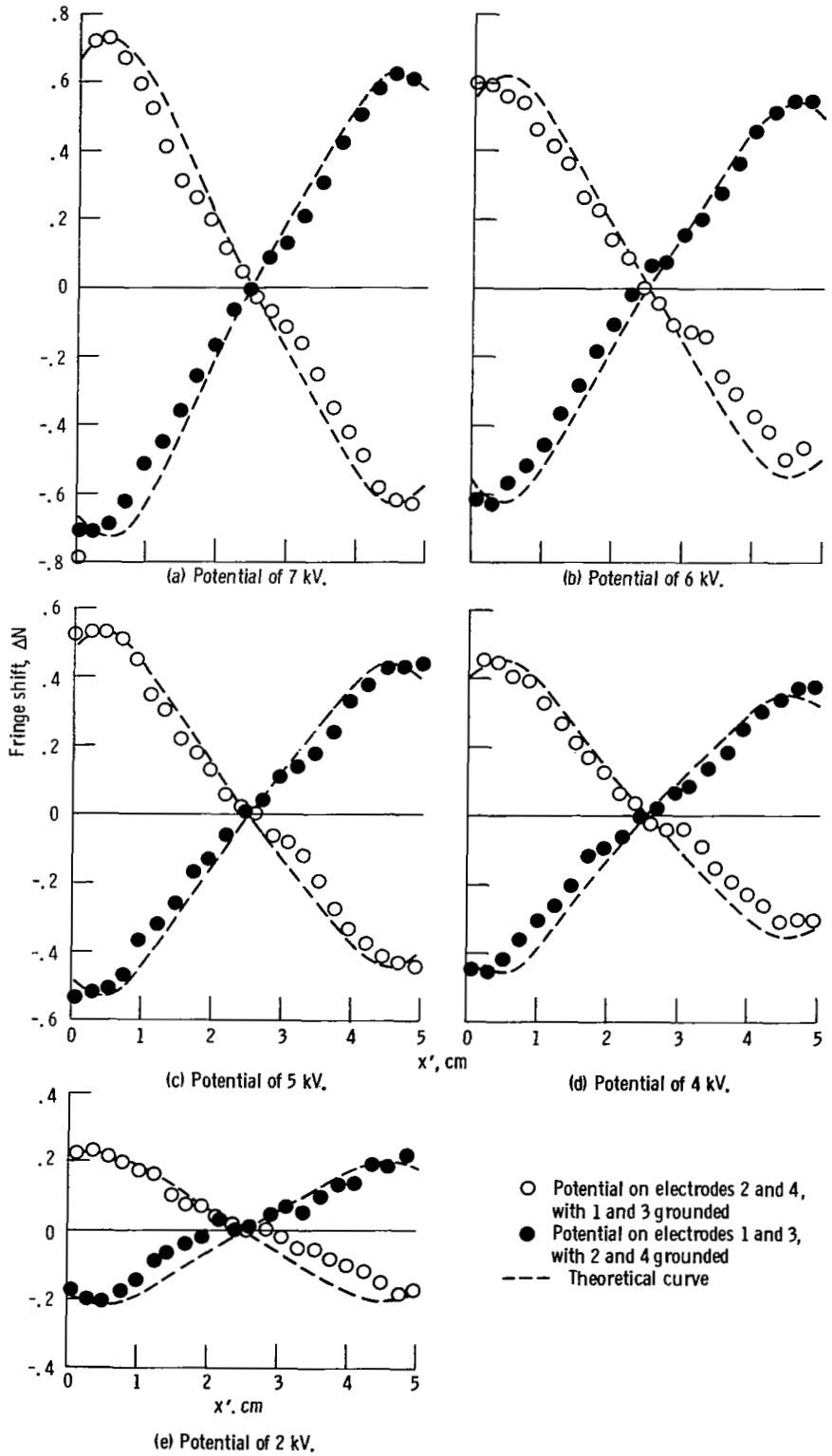

Figure 16. - Fringe shift for cut along centerline of crystal (z = 1.5 cm).

1. Report No.	2. Government Accession No.	3. Recipient's Catalog No.
NASA TP-2007		

4. Title and Subtitle	5. Report Date
POCKELS-EFFECT CELL FOR GAS-FLOW SIMULATION	May 1982
	6. Performing Organization Code 505-32-82

7. Author(s)	8. Performing Organization Report No.
David Weimer	E-1028
	10. Work Unit No.

9. Performing Organization Name and Address	11. Contract or Grant No.
National Aeronautics and Space Administration Lewis Research Center Cleveland, Ohio 44135	
	13. Type of Report and Period Covered
12. Sponsoring Agency Name and Address	Technical Paper
National Aeronautics and Space Administration Washington, D. C. 20546	14. Sponsoring Agency Code

15. Supplementary Notes

16. Abstract

A Pockels-effect cell using a 5×5×3 cm KD*P crystal has been developed to be used as a gas-flow simulator. Index-of-refraction gradients have been produced in the cell by the fringing fields of parallel-plate electrodes. Calibration curves for the device have been obtained for index-of-refraction gradients in excess of 2.5×10^{-4}/m.

17. Key Words (Suggested by Author(s))	18. Distribution Statement
Interferometry Holography Flow visualization Pockels effect	Unclassified - unlimited STAR Category 35

19. Security Classif. (of this report)	20. Security Classif. (of this page)	21. No. of Pages	22. Price*
Unclassified	Unclassified	17	A02

* For sale by the National Technical Information Service, Springfield, Virginia 22161

NASA-Langley, 1982